

## BATTERIES

**High-entropy mechanism to boost ionic conductivity**

Yan Zeng<sup>1†</sup>, Bin Ouyang<sup>1,2,3\*†</sup>, Jue Liu<sup>4</sup>, Young-Woon Byeon<sup>1</sup>, Zijian Cai<sup>1,2</sup>, Lincoln J. Miara<sup>5‡</sup>, Yan Wang<sup>5</sup>, Gerbrand Ceder<sup>1,2\*</sup>

Advances in solid-state batteries have primarily been driven by the discovery of superionic conducting structural frameworks that function as solid electrolytes. We demonstrate the ability of high-entropy metal cation mixes to improve ionic conductivity in a compound, which leads to less reliance on specific chemistries and enhanced synthesizability. The local distortions introduced into high-entropy materials give rise to an overlapping distribution of site energies for the alkali ions so that they can percolate with low activation energy. Experiments verify that high entropy leads to orders-of-magnitude higher ionic conductivities in lithium (Li)-sodium (Na) superionic conductor (Li-NASICON), sodium NASICON (Na-NASICON), and Li-garnet structures, even at fixed alkali content. We provide insight into selecting the optimal distortion and designing high-entropy superionic conductors across the vast compositional space.

**A** critical advancement in the development of superionic conductors for solid-state batteries has been the discovery of structural frameworks that provide connected low-barrier diffusion channels for facile ion migration (1–6). Recent progress in the development of Li-ion conductors has been largely driven by searching for frameworks with the right Li coordination environment (1, 2), Li site connectivity (3), distortion tolerance of the anion framework (4, 5), or crystalline symmetry (6). Several basic concepts have emerged to increase the alkali ion conductivity in compounds: (i) A percolating pathway of sites needs to exist along which coordination change is minimized. This is particularly important for sulfides in which the  $S^{2-}$  ion screens much of the electrostatic interaction between the carrier and the other cations. (ii) Raising the energy of the carrier ions increases their mobility. This can be achieved by increasing the amount of alkali ions in the compound (Li or Na “stuffing”), which forces the alkali to occupy higher-energy sites and/or raises their energy by increasing alkali-alkali repulsion. Alkali stuffing has been applied successfully to increase conductivity in  $Li_{1+x}Al_xTi_{2-x}(PO_4)_3$  (7) and  $Na_{3+x}Zr_2(SiO_4)_{2+x}(PO_4)_{1-x}$  in the Na superionic conductor (NASICON) framework (8) and  $Li_7La_3Zr_2O_{12}$  (LLZO) in the garnet framework (9). Although these concepts are valuable, the charge compensation needed to achieve a high alkali concentration may be associated

with a limited selection of possible dopants (10), complicated synthesis (3), and pronounced Li loss during heat treatment (11). We combined ab initio modeling and experiments to unveil how high entropy can affect ionic conductivity using nonstuffed common oxide-based frameworks.

Figure 1A illustrates our hypothesis of how local structural distortions can enhance alkali ion mobility. Consider a well-ordered structure with two distinct sites: Whereas site 1 has the lowest energy, site 2 can be an alkali-metal site within the diffusion network where the alkali ion has higher energy or it can be a high-symmetry saddle point along a hopping path. Introducing chemical disorder and its resulting distortions will locally perturb the site energy, creating a distribution of site energies. When this distribution is wide enough for the energy of neighboring sites to overlap, ion hopping between them will be promoted. If such a network of sites with similar energy percolates, macroscopic diffusion is enhanced by the disorder.

Using density functional theory (DFT), we quantified how structural distortions modify the energy of the alkali-metal sites in three common oxide-based ion conducting frameworks: Li-NASICON, Na-NASICON, and Li-garnet, starting from the baseline compounds  $LiTi_2(PO_4)_3$  (LTP),  $NaZr_2(PO_4)_3$  (NZP), and  $Li_3Nd_3Te_2O_{12}$  (LNTO). Gaussian-distributed local distortions with a standard deviation ( $d_o$ ) of 0.1 Å were applied to the metal-oxygen bond length in LTP (Ti-O), NZP (Zr-O), and LNTO (Nd-O and Te-O) at fixed supercell volume. A Gaussian was chosen for convenience, but any distribution that perturbs the site energy is expected to give qualitatively similar results. The site energy was probed by inserting a single alkali at the different sites of the framework and was properly charge-compensated with background charge (see materials and methods). Figure 1B shows the resulting energy distributions for the lowest- and highest-energy sites in each struc-

ture, with the site energy in the undistorted structure indicated by the dashed vertical lines. Taking LNTO as an example, the energy difference between the  $Li_{24d}$  and  $Li_{48g}$  sites is 1.57 eV, which establishes the minimum energy barrier for percolating ion hopping. The black and purple curves in Fig. 1B represent the site energies of these two sites in the distorted structures, showing a notable overlap between the energy distributions of both sites. This overlap is even more substantial in distorted LTP and NZP. Additional percolation analysis, including the  $Li_{36f}$  site in LTP, is shown in fig. S1.

We anticipate that the overlap in site energies provides a diffusion pathway along which the site-energy varies minimally (Fig. 1C). The connectivity of the pathway depends on the maximum site-energy difference that one allows between nearest neighbors ( $\Delta E_{NN}^{\max}$ ). Figure 1D shows the fraction of alkali sites that are part of the percolating trajectory for a given value of  $\Delta E_{NN}^{\max}$ . In the undistorted (ordered) LTP, percolation cannot occur until  $\Delta E_{NN}^{\max}$  reaches the energy difference between the 6b and 18e site (0.72 eV). For NZP and LNTO, the  $\Delta E_{NN}^{\max}$  are 0.85 and 1.57 eV, respectively. By contrast, when local bond distortion ( $d_o = 0.1$  Å) is introduced, percolation can occur at a much smaller  $\Delta E_{NN}^{\max}$ . Specifically, in distorted LTP, percolation with 24.2% of Li sites participating begins at  $\Delta E_{NN}^{\max} = 0.18$  eV, and more sites can percolate at higher  $\Delta E_{NN}^{\max}$ . In distorted NZP, 22.3% of Na sites form a percolation network at  $\Delta E_{NN}^{\max} = 0.14$  eV. In distorted LNTO, 5.2% of Li sites percolate at  $\Delta E_{NN}^{\max} = 0.39$  eV. Diffusion will occur through these percolation networks with a minimal activation energy equal to  $\Delta E_{NN}^{\max}$ . Hence, this basic analysis shows that disorder can result in a dramatic lowering of the alkali ion diffusion activation energy by creating a percolation network of sites with small energy differences.

We designed three nonstuffed high-entropy materials— $Li(Ti,Zr,Sn,Hf)_2(PO_4)_3$  (LTZSHPO),  $Na(Ti,Zr,Sn,Hf)_2(PO_4)_3$  (NTZSHPO), and  $Li_3(La,Pr,Nd)_3(Te,W)_2O_{12}$  (LLPNTWO)—to represent the Li-NASICON, Na-NASICON, and Li-garnet frameworks, respectively. Higher-entropy materials enable the joint solubility of ions with a large ionic radius difference, which will create the bond-length deviations that are shown by our analysis to enhance diffusion.

Figure 2A shows the x-ray diffraction (XRD) patterns of LTZSHPO, NTZSHPO, and LLPNTWO that were synthesized by a solid-state reaction. By indexing to the reference patterns, we find that LTZSHPO and NTZSHPO form the rhombohedral  $R\bar{3}c$  NASICON structure, whereas LLPNTWO forms the cubic  $Ia\bar{3}d$  garnet structure. There are no visible impurity peaks in the three patterns, which indicates single-phase samples. Rietveld refinements

<sup>1</sup>Materials Sciences Division, Lawrence Berkeley National Laboratory, Berkeley, CA 94720, USA. <sup>2</sup>Department of Materials Science and Engineering, University of California Berkeley, Berkeley, CA 94720, USA. <sup>3</sup>Department of Chemistry and Biochemistry, Florida State University, Tallahassee, FL 32304, USA. <sup>4</sup>Neutron Scattering Division, Oak Ridge National Laboratory, Oak Ridge, TN 37831, USA. <sup>5</sup>Advanced Materials Lab, Samsung Advanced Institute of Technology—America, Samsung Semiconductor Inc., Cambridge, MA 02138, USA. \*Corresponding author: Email: bouyang@fsu.edu (B.O.); gceder@berkeley.edu (G.C.).

†These authors contributed equally to this work.

‡Present address: Pure Lithium Corporation, Charlestown, MA 02129, USA.

**Fig. 1. Effect of structural distortions on alkali site energies and percolation.** (A) Schematic showing how local distortions create overlapping site-energy distributions. (B) Calculated site energies before (dashed vertical lines) and after introducing a standard deviation of  $0.1 \text{ \AA}$  to the metal-oxygen bond lengths in three baseline materials. (C) Schematic of percolation defined as the network of sites in which the maximum nearest-neighbor site-energy difference is  $\Delta E_{\text{NN}}^{\text{max}}$ . (D) Calculated fraction of percolating Li or Na sites as a function of  $\Delta E_{\text{NN}}^{\text{max}}$  in distorted (solid lines) and undistorted (dashed lines) structures. The arrows point out the lowest  $\Delta E_{\text{NN}}^{\text{max}}$  at which percolation occurs.

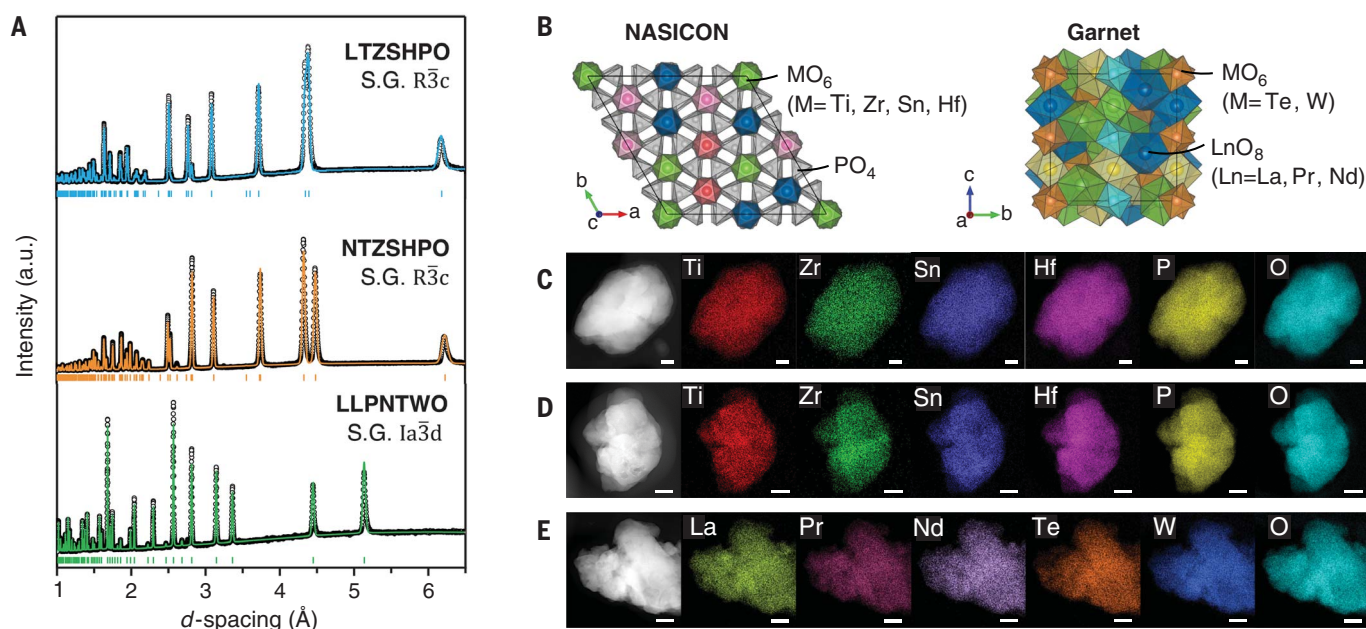
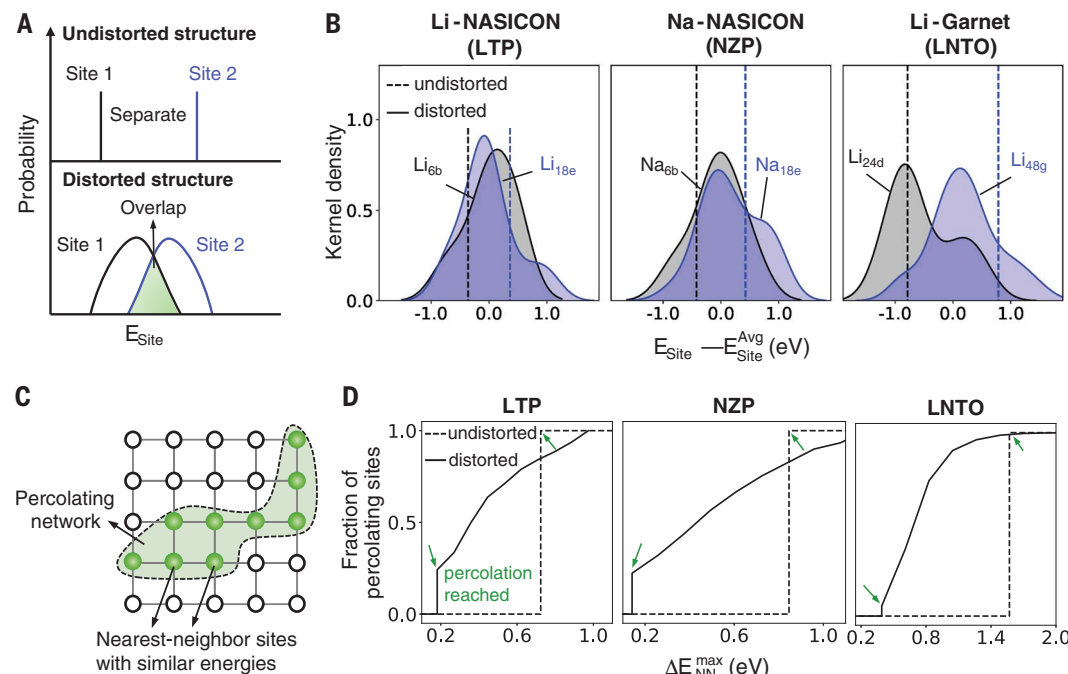


**Fig. 2. Synthesis and structures of three high-entropy oxides.** (A) XRD patterns (open circles, observed; solid lines, calculated; sticks, Bragg positions) of NASICON and garnet-based high-entropy materials. a.u., arbitrary units. (B) Schematics of the NASICON and garnet structures with multiple

elements substituting on one site. Li and Na are not shown. (C to E) HAADF-STEM images and elemental mappings of LTZSHPO (C), NTZSHPO (D), and LLPNTWO (E), showing that the elements are homogeneously distributed. Scale bars are 50 nm.

indicate a good fit when Ti, Zr, Sn, and Hf are distributed on the octahedral MO<sub>6</sub> site (Fig. 2B). For LLPNTWO, La, Pr, and Nd are confirmed to share the dodecahedral LnO<sub>8</sub> site, whereas Te and W share the octahedral MO<sub>6</sub> site (Fig. 2B). Energy-dispersive x-ray (EDX) spectroscopy from a high-angle annular dark-field scanning transmission electron

microscope (HAADF-STEM) (Fig. 2, C to E) shows that each element is uniformly distributed, which provides further evidence that no impurity phases exist.

The ionic conductivities of the three high-entropy materials were determined by electrochemical impedance spectroscopy (Fig. 3A). The overall room-temperature conductivities

are  $2.2 \times 10^{-5} \text{ S/cm}$  for LTZSHPO (15% porosity),  $1.2 \times 10^{-6} \text{ S/cm}$  for NTZSHPO (20% porosity), and  $1.7 \times 10^{-6} \text{ S/cm}$  for LLPNTWO (27% porosity). Figure 3A also presents the conductivities of the single-metal analog compounds that were synthesized and measured using the same approaches as the high-entropy samples. The ionic conductivities of all three high-entropy

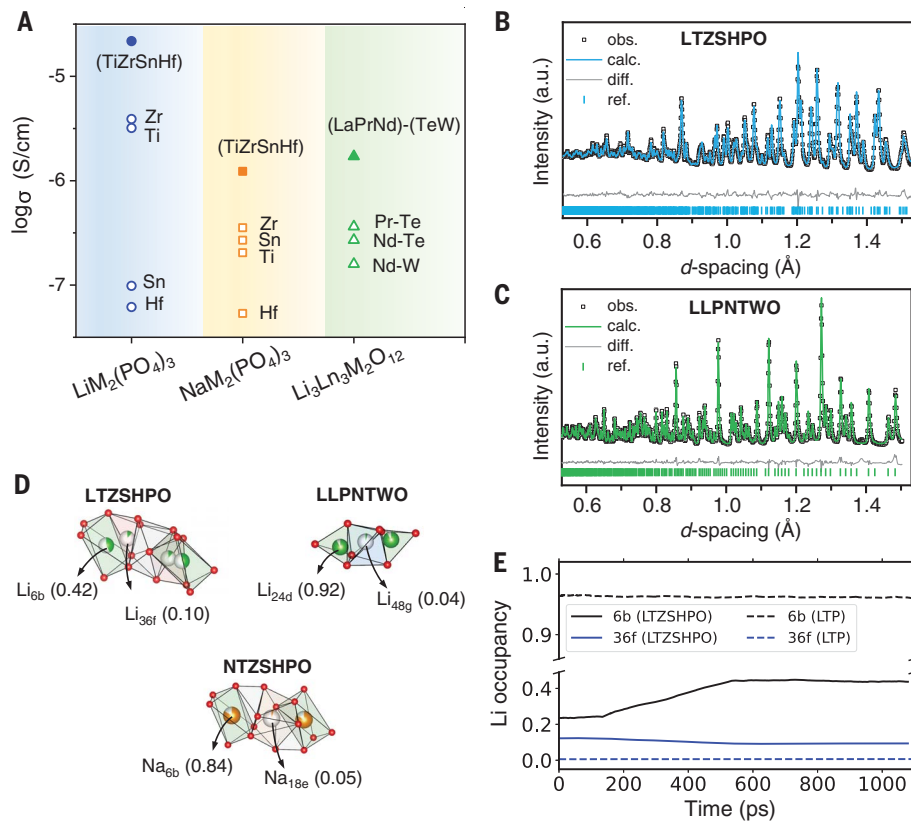


**Fig. 3. Ionic conductivities and Li or Na occupancies for the high-entropy materials.** (A) Ionic conductivities of LTZSHPO, NTZSHPO, and LLPNTWO and their single-metal counterparts measured at room temperature. (B and C) Neutron diffraction patterns and refinements of LTZSHPO (B) and LLPNTWO (C). obs., observed; calc., calculated; diff., difference; ref., reference. (D) Schematics of Li or Na partial occupancies determined from neutron diffraction or XRD refinements.  $\text{Li}_{6b}$  (0.42) designates that the occupancy factor of Li on 6b sites is 0.42. (E) AIMD-simulated Li-site occupancy evolution in LTZSHPO (solid lines) and LTP (dashed lines) at 300 K.

materials surpass those of their single-metal counterparts by several orders of magnitude (figs. S2 to S5 and table S1).

We attribute the enhancement of ionic conductivity in the high-entropy materials to the cation disorder that creates site-energy overlap and promotes ion percolation (Fig. 1). To acquire more explicit experimental evidence of Li disorder across sites, we assessed the Li site occupancies through refinement of time-of-flight neutron diffraction patterns (Fig. 3, B and C). In LTZSHPO, the site occupancy factors (SOF) found are  $\text{SOF}(\text{Li}_{6b}) = 0.4182$  and  $\text{SOF}(\text{Li}_{36f}) = 0.0970$  (illustrated in Fig. 3D). As a comparison, LTP contains Li exclusively on 6b sites (fig. S6). Moreover, other single-metal  $\text{LiM}_2(\text{PO}_4)_3$  have not been observed to exhibit Li partial occupancy at room temperature (12–14). We also observed partial occupancies in the garnet LLPNTWO with  $\text{SOF}(\text{Li}_{24d}) = 0.9196$  and  $\text{SOF}(\text{Li}_{48g}) = 0.0402$  (Fig. 3D). In comparison, LNTO contains Li exclusively on 24d sites (fig. S6). Other low-entropy Li<sub>3</sub>-garnets also only accommo-

date Li on 24d sites (15). We obtained the Na site occupancy factor for NTZSHPO from XRD to be  $\text{SOF}(\text{Na}_{6b}) = 0.8383$  and  $\text{SOF}(\text{Na}_{18e}) = 0.0539$  (Fig. 3D). Again, single-metal  $\text{NaM}_2(\text{PO}_4)_3$  only accommodates Na on 6b sites (16, 17). The detailed Rietveld refinements are presented in tables S2 to S4. These observations confirm that multiple metals on cation sites create Li- or Na-site disorder, which can only arise when their otherwise distinct sites become more similar in energy.

To further validate that high-entropy materials have a stronger tendency to create Li-site disorder than their single-metal analogs, we performed ab initio molecular dynamics (AIMD) simulations to compare LTZSHPO and LTP in the canonical ensemble at 300 K (see methods). The site occupancy evolution along a 1.1-ns trajectory of AIMD simulations is demonstrated in Fig. 3E. The occupancy versus time shown in Fig. 3E was calculated by averaging the occupancies in a trajectory during the past 100 ps. Figure 3E shows that the average Li occupancies in LTZSHPO grad-

ually converge to 0.40 on 6b sites and 0.09 on 36f sites after around 0.6 ns, close to the experimental observations (Fig. 3B). By contrast, there is barely any site occupancy change for LTP. This simulation confirms the higher disordering tendency in LTZSHPO compared with that in LTP.

Unlike many other physical properties of materials, diffusivity is not an “averaged” property over the structure. The ionic conductivity in materials does not depend on the average migration rate between all pairs of sites but rather depends on the fastest percolating pathway the ions can take through the system. Because of the very high connectivity of sites in a typical crystal structure (many paths can be created between two distant sites), ion transport is not sensitive to some of these paths being very high in energy, because an ion variationally picks the path of lowest resistance. This explains why the site-energy distributions that are created through the high-entropy metal cation disorder are so effective for promoting percolation. It creates a sufficient probability that some neighboring sites are close in energy, making it easier for ions to jump between them. At a critical level of such close-energy neighbors, the system percolates and has high conductivity. The fact that disorder may also create nearest-neighbor site pairs with an increased energy difference does not matter because their participation in transport is not required.

A small fraction of conductors may not benefit from high-entropy optimization. Purely one-dimensional (1D) conductors only have a single path available between two sites in the same channel (18), and perturbations to the site-energy landscape can lower conductivity by creating some high-energy barriers that need to be crossed. But for most materials that have 2D and 3D site connectivity, high entropy is a valid strategy to increase conductivity.

With these insights, we anticipate three scenarios for the site-energy distributions that arise from different degrees of distortion. When the distortion is minimal, or the site energies are too far apart, the dispersion of site energies created by local distortions is too narrow to create overlap between the two sites. Consequently, the alkali metals’ percolation can barely occur. At the other extreme, overly large distortions lead to a very broad dispersion of site energies, which increases the probability for neighboring sites to have a higher energy difference, thereby limiting ion percolation. Between these two extremes, there is an optimal range of distortion that creates a percolating network of sites that are all within a narrow energy range.

To put this in the context of real materials, Fig. 4A shows the calculated site-energy distributions in distorted LTP, NZP, and LNTO

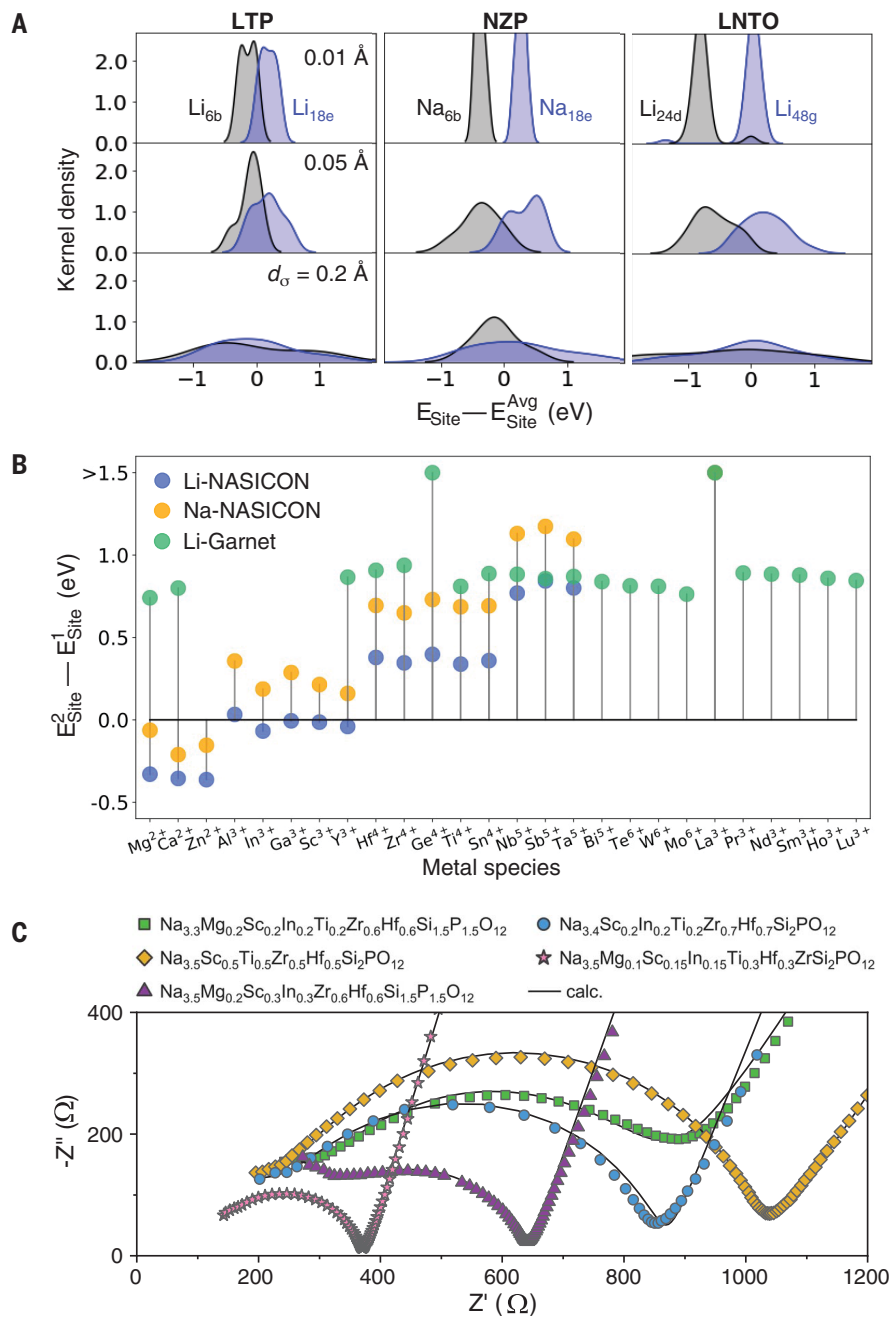


**Fig. 4. Design guidelines for optimal distortion and effect of metal chemistry.** (A) Calculated site-energy distributions in LTP, NZP, and LNTO with small ( $0.01 \text{ \AA}$ ), medium ( $0.05 \text{ \AA}$ ), and large ( $0.2 \text{ \AA}$ ) distortions. (B) Calculated site-energy difference with various metal species in Li-NASICON, Na-NASICON, and Li-garnet. For Li- and Na-NASICONs, site 1 refers to 6b sites and site 2 refers to 18e sites. For Li-garnet, site 1 refers to 24d sites and site 2 refers to 48g sites. (C) Nyquist plots of Na-stuffed high-entropy compounds.  $Z'$ , the real part of the impedance;  $-Z''$ , the imaginary part of the impedance.

with small ( $0.01 \text{ \AA}$ ), medium ( $0.05 \text{ \AA}$ ), and large ( $0.2 \text{ \AA}$ ) distortions, in addition to the  $0.1 \text{ \AA}$  that was used to generate Fig. 1B. We find that with  $d_{\sigma} = 0.01 \text{ \AA}$ , the energy of the two sites has no (e.g., NZP) or scarce (e.g., LTP and LNTO) overlap, whereas larger  $d_{\sigma}$  values ( $0.05 \text{ \AA}$  in Fig. 4B and  $0.1 \text{ \AA}$  in Fig. 1B) create more

overlap. However, a further increase of distortion ( $0.2 \text{ \AA}$ ) spreads out the site energies too much, making percolation difficult (percolation analysis in fig. S7). These results indicate that there is an optimal distortion for good ionic conductivity due to the trade-off between site-energy overlap and the amount of accessible percolating sites. Using DFT on a large supercell (fig. S8) with a random arrangement of the nonalkali metals, we found the bond-length deviation to be  $0.067 \text{ \AA}$  in LTZSHPO,  $0.065 \text{ \AA}$  in NTZSHPO, and  $0.054 \text{ \AA}$  in LLPNTWO (fig. S9), which creates overlapping site-energy distributions that are consistent with our explanation for the improved conductivity (fig. S10).

In addition to the structural distortions that can influence the alkali energy landscape, a direct interaction between the metal cations and the alkali ion may also modify the site energies (19). To probe this effect, we calculated how the site-energy difference varies with chemistry by substituting nonalkali metal cations in LTP, NZP, and LNTO. In this calculation, the atomic positions and lattice constants are fixed to separate the effect of chemistry from that of the distortion that was previously discussed. Figure 4B depicts the calculated site-energy difference in the presence of different metal species. Note that there are two different metal sites in Li-garnet, and the values in Fig. 4B are averaged from all compositions that have the targeted metal cation. Calculations for each individual composition are demonstrated in fig. S11. In Li-NASICON and Na-NASICON, the nonalkali metal cations can change the site-energy difference. In general, lower-valent metals (e.g.,  $\text{Mg}^{2+}$ ) prefer the alkali in 18e sites, whereas higher-valent metals (e.g.,  $\text{Zr}^{4+}$ ) in the compound stabilize the alkali in 6b. For garnets, although 24d sites are always preferred, the site-energy difference still varies. For example, the site-energy difference in garnet with  $\text{Pr}^{3+}$  or  $\text{Nd}^{3+}$  is more than 500 meV less than that with  $\text{La}^{3+}$ .

The entropy-stabilization mechanism of high-entropy compounds enables the solubility of more and different cations than would be possible under low-entropy conditions (20). This can be used to create site-energy distributions that lead to percolating transport networks with much higher ionic conductivity than those achieved with a single-metal cation component. Although in our work only a few compositions were tested, the high-dimensional nature of the high-entropy systems creates a vast opportunity space for compositional tuning and makes it more likely to stay within the space of earth-abundant and inexpensive elements. As demonstrated in our experiments and computations, high-entropy materials do not necessarily need an excess concentration of Li or Na to improve ionic conductivity, which may in turn help overcome the Li loss issues observed during the sintering of Li-stuffed ionic conductors (11) (also see table S5 for Li-loss in Li-garnets). To further this field, understanding is needed on which elements can form a compatible high-entropy ensemble through high-throughput modeling (10, 21) and rapid experimentation (22). For example, we found that

the NASICONs with five equimolar M<sup>4+</sup> metal cations (Ge, Ti, Zr, Sn, Hf) could not be synthesized, probably because of the large size mismatch of Ge<sup>4+</sup> with the other metal cations. Similarly, garnets with three equimolar M<sup>6+</sup> (Mo, W, Te) were attempted but did not lead to phase-pure samples.

The high-entropy strategy can potentially be combined with the alkali metal-stuffing strategy to further optimize the ionic conductivity. To support this idea, we designed and synthesized five Na-stuffed high-entropy NASICON compounds (XRD in fig. S12). The measured impedance spectra are plotted in Fig. 4C, with detailed information provided in fig. S13 and table S1. All five compounds exhibit bulk room-temperature ionic conductivities that exceed 1 mS/cm. Na<sub>0.5</sub>Mg<sub>0.1</sub>Sc<sub>0.15</sub>In<sub>0.15</sub>Ti<sub>0.3</sub>Hf<sub>0.2</sub>ZrSi<sub>2</sub>PO<sub>12</sub>, even with 7% pellet porosity, shows a total conductivity of 1.1 mS/cm and a bulk conductivity of 3.3 mS/cm, which is comparable to that of the fastest Na-ion conductors (10, 23).

We demonstrate that the local disorder in high-entropy materials can effectively promote site percolation and enhance ionic conductivity through the creation of overlapping site-energy distributions. This work paves the way for developing high-entropy superionic conductors and a pathway to achieve high ionic conductivity in solid electrolytes and other applications involving ion diffusion.

## REFERENCES AND NOTES

- X. He et al., *Adv. Energy Mater.* **9**, 1902078 (2019).
- Y. Wang et al., *Nat. Mater.* **14**, 1026–1031 (2015).
- Y. Xiao et al., *Adv. Energy Mater.* **11**, 2101437 (2021).
- D. Di Stefano et al., *Chem* **5**, 2450–2460 (2019).
- K. Jun et al., *Nat. Mater.* **21**, 924–931 (2022).
- Y. Zhang et al., *Nat. Commun.* **10**, 5260 (2019).
- H. Aono, E. Sugimoto, Y. Sadaoka, N. Imanaka, G. y. Adachi, *J. Electrochem. Soc.* **137**, 1023–1027 (1990).
- H. Y. P. Hong, *Mater. Res. Bull.* **11**, 173–182 (1976).
- M. P. O'Callaghan, A. S. Powell, J. J. Titman, G. Z. Chen, E. J. Cussen, *Chem. Mater.* **20**, 2360–2369 (2008).
- B. Ouyang et al., *Nat. Commun.* **12**, 5752 (2021).
- A. Paoletta et al., *ACS Appl. Energy Mater.* **3**, 3415–3424 (2020).
- E. R. Losilla, M. A. G. Aranda, M. Martínez-Lara, S. Brueque, *Chem. Mater.* **9**, 1678–1685 (1997).
- M. Catti, S. Stramare, R. Ibberson, *Solid State Ion.* **123**, 173–180 (1999).
- E. I. Morin et al., *ChemInform* **29**, 1 (1997).
- M. P. O'Callaghan, D. R. Lynam, E. J. Cussen, G. Z. Chen, *Chem. Mater.* **18**, 4681–4689 (2006).
- J. Alamo, J. L. Rodrigo, *Mater. Res. Bull.* **27**, 1091–1098 (1992).
- G. Pang et al., *Nanoscale* **6**, 6328–6334 (2014).
- D. Morgan, A. Van der Ven, G. Ceder, *Electrochim. Solid-State Lett.* **7**, A30 (2004).
- D. A. Kuznetsov et al., *Joule* **2**, 225–244 (2018).
- C. Oses, C. Toher, S. Curtarolo, *Nat. Rev. Mater.* **5**, 295–309 (2020).
- Z. Lun et al., *Nat. Mater.* **20**, 214–221 (2021).
- N. J. Szymanski et al., *Mater. Horiz.* **8**, 2169–2198 (2021).
- Y. Tian et al., *Chem. Rev.* **121**, 1623–1669 (2021).

## ACKNOWLEDGMENTS

**Funding:** This work was supported by the Assistant Secretary for Energy Efficiency and Renewable Energy, Vehicle Technologies

Office, of the US Department of Energy under contract no. DE-AC02-05CH1231. The computational analysis was performed using Eagle and Swift at the National Renewable Energy Laboratory, Extreme Science and Engineering Discovery Environment, supported by NSF ACI1053575; and the National Energy Research Scientific Computing Center. Neutron diffraction was conducted at the NOMAD beamlines at Oak Ridge National Laboratory's Spallation Neutron Source, which was sponsored by the Scientific User Facilities Division, whereas STEM was performed at the National Center for Electron Microscopy (NCEM) at Lawrence Berkeley National Laboratory (LBNL). Both facilities are supported by the Office of Science of the US Department of Energy. We also appreciate K. Bustillo from NCEM at LBNL for her technical assistance in STEM. **Author contributions:** Y.Z., B.O., and G.C. planned this work. G.C. supervised all aspects of the research. Y.Z. synthesized, characterized, and tested the proposed materials. Y.Z. and B.O. proposed and designed the theoretical calculations. B.O. performed the calculations and analyzed the results with help from Y.W. J.L. collected and helped Y.Z. analyze the neutron diffraction data. Y.-W.B. performed STEM. Z.C. performed inductively coupled plasma. Y.Z., B.O., and G.C. wrote the paper with help from L.J.M. All authors contributed to discussions and writing. **Competing interests:** None declared.

**Data and materials availability:** All data are available in the paper and the supplementary materials. **License information:** Copyright © 2022 the authors, some rights reserved; exclusive licensee American Association for the Advancement of Science. No claim to original US government works. <https://www.science.org/about/science-licenses-journal-article-reuse>

## SUPPLEMENTARY MATERIALS

[science.org/doi/10.1126/science.abq1346](https://science.org/doi/10.1126/science.abq1346)  
Materials and Methods  
Figs. S1 to S13  
Tables S1 to S5  
References (24–27)

Submitted 20 March 2022; accepted 28 October 2022  
[10.1126/science.abq1346](https://science.org/10.1126/science.abq1346)

## High-entropy mechanism to boost ionic conductivity

Yan ZengBin OuyangJue LiuYoung-Woon ByeonZijian CaiLincoln J. MiaraYan WangGerbrand Ceder

Science, 378 (6626), • DOI: 10.1126/science.abq1346

### High entropy by design

A key property for solid-state battery electrolytes is the ability to rapidly transport lithium ions. This property can be achieved by developing a percolating pathway or by increasing the mobility of the carrier ions in the electrolyte. However, standard design methods limit the selection of dopants and complicate the synthesis. Zeng *et al.* adapted some of the concepts of high-entropy materials to the development of solid electrolytes (see the Perspective by Botros and Janek). The addition of a mixture of high-entropy metal cations induces local disorder, thus creating overlapping site energy distributions for charge-carrying ions. This approach results in a percolating network of connected sites with a reduced energy difference and correspondingly fast lithium ion transport, as demonstrated for lithium- and sodium-based batteries. —MSL

### View the article online

<https://www.science.org/doi/10.1126/science.abq1346>

### Permissions

<https://www.science.org/help/reprints-and-permissions>